

# Nonlinear Evolution of the Lower-hybrid Drift Instability in a Current Sheet

William Daughton<sup>1</sup>, Giovanni Lapenta<sup>1,2</sup>, and Paolo Ricci<sup>1,2</sup>

<sup>1</sup>*Los Alamos National Laboratory, Los Alamos, New Mexico 87545 and*

<sup>2</sup>*Istituto Nazionale per la Fisica della Materia (INFN), Sezione di Torino, Italy*

(Dated: April 18, 2004)

The evolution of an ion-scale current sheet is simulated with a fully kinetic approach using values of the ion to electron mass ratio up to  $m_i/m_e = 1836$ . Although the lower-hybrid drift instability is localized in the edge region, the nonlinear development strongly modifies the electron flow velocity in the central region, which induces a bifurcation of the current density and leads to anisotropic heating of the electron distribution. The essential physics involves a resonant scattering of crossing ion orbits into the noncrossing regime of phase space which creates an electrostatic potential structure across the layer. These modifications dramatically enhance the collisionless tearing mode leading to the rapid onset of magnetic reconnection for current sheets near the critical scale.

PACS numbers: 52.35.Vd, 94.30.Ej, 94.30.Gm, 52.35.Kt

Current sheets with characteristic thickness on the order of a thermal ion gyroradius  $\rho_i$  are routinely observed in the Earth's magnetosphere [1, 2] and within laboratory experiments designed to examine the physics of magnetic reconnection [3], a topic with widespread application to space, astrophysical and laboratory plasmas. Although current sheets are unstable to a variety of plasma instabilities including collisionless tearing [4] and the lower-hybrid drift instability [5], the relative importance of these instabilities to the onset and development of large scale magnetic reconnection remains controversial.

The lower-hybrid drift instability (LHDI) is driven by the diamagnetic current in the presence of inhomogeneities in the density and magnetic field [6]. The LHDI has been considered extensively as a possible candidate to modify the reconnection physics through anomalous resistivity generated by wave-particle interactions [5, 7, 8]. Unfortunately, theory predicts the fastest growing modes with wavelength on the electron gyroscale  $k_y \rho_e \sim 1$  are localized on the edge of the layer [5], while enhanced fluctuations are required in the central region to produce significant anomalous resistivity. This conclusion is supported by observations at the magnetopause [9], in the magnetotail [10] and by laboratory experiments [11].

Based on this evidence, some researchers have concluded the LHDI does not play an important role in current sheet dynamics. However, new results from both theory and simulation are beginning to challenge this conclusion. In a number of simulations, a strong enhancement of the central current density associated with the LHDI is observed [12–15] and it has been suggested this effect gives rise to the rapid onset of reconnection [14]. Most of these simulations were performed with artificial ion to electron mass ratios  $m_i/m_e \approx 100 - 256$  and very thin layers  $\rho_i/L \approx 1.7 - 2.2$ , where  $L$  is the half thickness of the layer. Although the simulations in Ref. [13] considered thicker layers at realistic mass ratio, the focus was on long wavelength effects and the spatial resolution was insufficient to resolve the full LHDI spectrum.

The very thin layers considered in most of the simulations are comparable in thickness to laboratory recon-

nection experiments [3, 16] but are considerably thinner than observed in the magnetotail prior to onset. In this regime, kinetic simulations indicate significant penetration of electromagnetic fluctuations into the central region [7, 8, 12]. An explanation for these waves was recently proposed based on a new approach to the linear stability [17] which predicts the longer wavelength LHDI with  $k_y \sqrt{\rho_i \rho_e} \sim 1$  can penetrate into the central region even though the fastest growing modes with  $k_y \rho_e \sim 1$  are confined to the edge. The required thickness for this penetration [17] is approximately  $\rho_i/L \gtrsim 1.5$ .

In the magnetotail, the observed thickness of the current sheet [1] is larger  $\rho_i/L \lesssim 1$  and it appears the LHDI is well localized on the edge. In this work, the nonlinear evolution of the LHDI is examined for this regime using a two-dimensional (2D) kinetic approach with the physical value of the mass ratio for a hydrogen plasma  $m_i/m_e = 1836$  and fully resolving all relevant spatial and temporal scales. The nonlinear development leads to a rich variety of interesting new physics including a strong bifurcation of the current density and significant anisotropic heating of the electron distribution in the central region. Furthermore, a simple physics model is proposed which can explain both of these features. These new results may have direct relevance in understanding bifurcated current sheets recently observed in the magnetotail [18, 19]. In addition, these modifications to the current sheet structure greatly enhance the growth rate of the collisionless tearing mode and may play a crucial role in determining the onset of large scale reconnection [20].

The initial configuration is a Harris sheet [21] with magnetic field  $B_x = B_o \tanh(z/L)$  and plasma current  $J_y = J_o \text{sech}^2(z/L)$ . The initial distributions are drifting Maxwellians with thermal velocity  $v_{th_s} \equiv (2T_s/m_s)^{1/2}$  and uniform drift  $U_s = 2cT_s/(q_s B_o L)$  where  $T_s$  is the temperature,  $m_s$  is the mass,  $q_s$  is the charge, the density profile is  $n(z) \equiv n_o \text{sech}^2(z/L)$  and  $s = i, e$  for ions and electrons. In addition, a spatially uniform background distribution with zero drift velocity is included, since the stability properties of the LHDI are sensitive to this feature [17]. The dimensionless equilibrium parameters are

$\rho_i/L = 1$ ,  $T_i/T_e = 5$ ,  $\omega_{pe}/\Omega_{ce} = 4$ ,  $n_b/n_o = 0.02$ , where  $\rho_i = v_{thi}/\Omega_{ci}$  is an ion gyroradius,  $\Omega_{cs} = eB_o/(m_s c)$  is the gyrofrequency computed from the asymptotic field  $B_o$ ,  $\omega_{pe} = (4\pi n_o e^2/m_e)^{1/2}$  is the plasma frequency calculated from the peak density  $n_o$  and  $n_b$  is the background density which is loaded as a uniform Maxwellian with temperature  $T_b = T_e$ . These parameters are roughly appropriate for conditions observed in the magnetotail [1, 22]. Simulations were performed for two different mass ratios:  $m_i/m_e = 1836$  to simulate realistic conditions over a short duration and  $m_i/m_e = 512$  to examine the nonlinear evolution over a longer period.

The 2D kinetic simulations are based on a well-known explicit electromagnetic algorithm [23, 24] in which the fields are advanced using the scalar and vector potentials. Working in the Coulomb gauge, the scalar potential is computed directly from Poisson's equation, while the vector potential is advanced in time using a semi-implicit method which permits the time step to exceed the Courant limit [24]. For waves with phase velocity much less than the speed of light, this approach is very accurate and comparisons against a fully explicit method [23] have revealed no significant differences. The boundary conditions for the particles and fields are periodic in the  $y$  direction. Conducting boundary conditions are imposed for the fields at the  $z$  boundaries while reflecting boundary conditions are used for the particles. In both simulations, the box size is  $12L \times 12L$  and the time step is  $\Delta t \Omega_{ce} = 0.1$  which fully resolves the electron motion but is approximately 6 times faster than the Courant limit. For  $m_i/m_e = 1836$ , the spatial grid is  $5120 \times 5120$  with  $6 \times 10^9$  particles while for  $m_i/m_e = 512$ , the spatial grid is  $2560 \times 2560$  with  $1.6 \times 10^9$  particles.

At the physical mass ratio, the fastest growing mode from a linear Vlasov calculation [17] has wavelength  $k_y \rho_e \approx 0.5$  with real frequency  $\omega/\Omega_{ci} \approx 27.9$ , growth rate  $\gamma/\Omega_{ci} \approx 5.7$  and is localized in the region  $0.7 \lesssim |z/L| \lesssim 2$ . These predictions are in excellent agreement with the simulation results and fluctuations are well confined to the edge. Since the LHDI is driven by the diamagnetic drifts, one would expect a reduction of these drifts and consequently a reduction in the current density in the region of LHDI activity. This expectation is confirmed in Fig. 1a for the simulation with  $m_i/m_e = 1836$ . The surprising result is the pronounced off-axis current filaments near  $z/L \approx 0.20$ . The modified current profile is largely due to changes in the electron fluid velocity  $V_{ey}$  as shown in Fig 1b while changes in the ion fluid velocity and density are relatively minor. In addition, the electrons are heated in the direction perpendicular to the magnetic field resulting in a non-Maxwellian distribution in the central region. A rough estimate of these non-Maxwellian features is given in terms of the electron anisotropy  $T_{e\perp}/T_{e\parallel}$  in Fig. 1c. However, it should be emphasized that a more careful examination has revealed the electron distribution has significant non-gyrotropic features in this region. At first glance, the results in Fig. 1 are perplexing since there is no wave activity in the

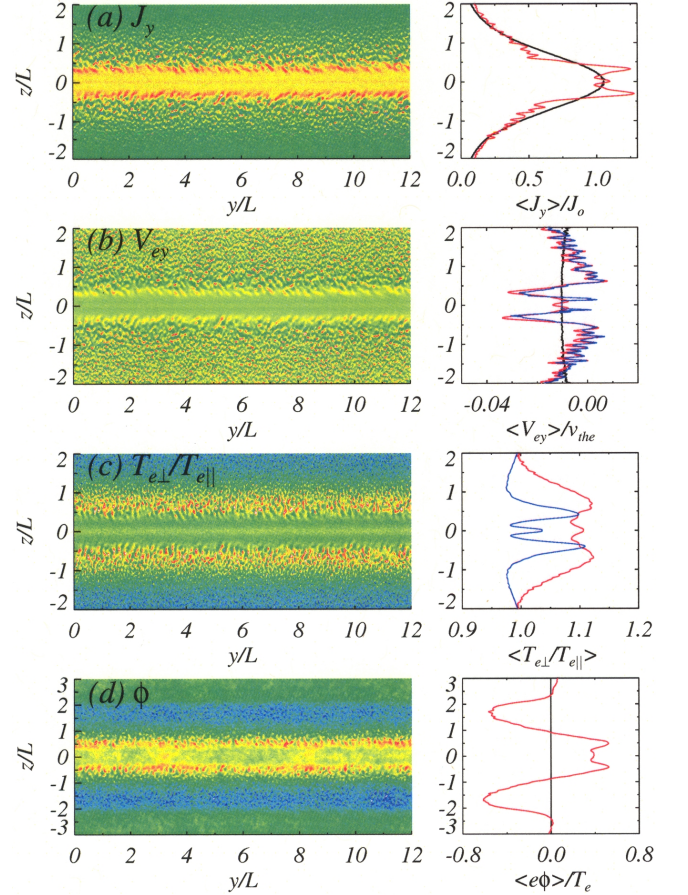


FIG. 1: Simulation results for  $m_i/m_e = 1836$  at time  $t\Omega_{ci} = 7$  showing (a) current density  $J_y$ , (b) electron fluid velocity  $V_{ey}$ , (c) electron anisotropy  $T_{e\perp}/T_{e\parallel}$  and (d) electrostatic potential  $\phi$ . Contours of each quantity are shown on the left, while the  $y$ -average is shown on the right (red) along with the initial profile (black). The blue line in (b) corresponds to the  $y$ -average of the prediction for  $V_{ey}$  in Eq. (2), while the blue line in (c) corresponds to the anisotropy estimate in Eq. (3).

region  $|z/L| \lesssim 0.7$ . Nevertheless, a fairly simple physics model is sufficient to explain all of these results.

The constants of motion for a charged particle moving in the equilibrium field are  $\varepsilon = m_s(v_z^2 + v_y^2)/2$ ,  $v_x$  and  $p_y = m_s v_y + q_s A_y/c$  where  $A_y$  is the vector potential  $A_y = -B_o L \ln[\cosh(z/L)]$  for the Harris field. Particles with  $\varepsilon > p_y^2/2m_s$  traverse both sides of the current layer and are referred to as *crossing* trajectories while particles with  $\varepsilon < p_y^2/2m_s$  are confined to one side of the layer and are referred to as *noncrossing*. The boundary between crossing and noncrossing regions of phase space is

$$\frac{v_y}{v_{ths}} = \frac{\alpha}{2} - \frac{1}{2\alpha} \left( \frac{v_z}{v_{ths}} \right)^2, \quad (1)$$

where  $\alpha = (L/\rho_s) \ln[\cosh(z/L)]$ . An example cross-section of phase space is illustrated in Fig. 2, for the region of the sheet with strong LHDI fluctuations. The parabolic curves correspond to Eq. (1) at the spatial posi-

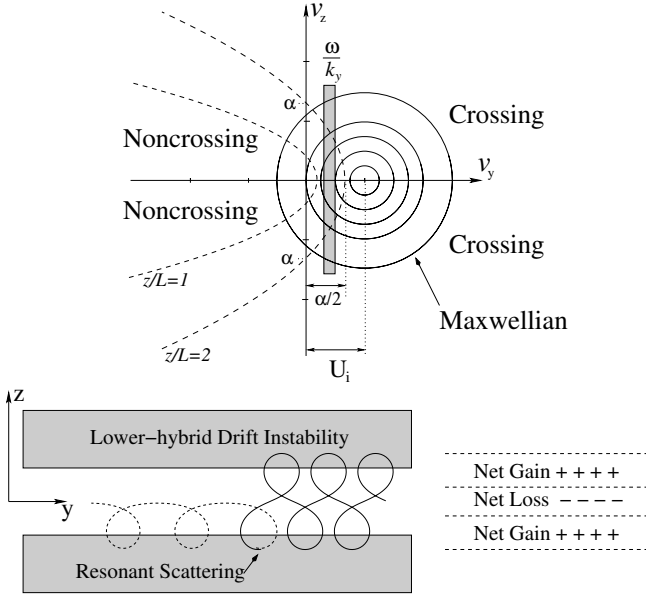


FIG. 2: Cross section of phase space (top) in the  $v_z - v_y$  plane illustrating a drifting Maxwellian ion distribution and the phase space boundary in Eq. (1) for two different spatial positions within the layer. The shaded region in the upper figure corresponds to the approximate phase velocity of the waves  $\omega/k_y \approx U_i/2$  which are in the proper region to resonantly scatter crossing ions into the noncrossing region of phase space. This scattering process and the resulting charge accumulation is illustrated in the lower figure.

tions  $z/L = 1, 2$  while the concentric circles correspond to the Maxwellian ion distribution. The phase space boundary is the only feature which varies with spatial position in Fig. 2 since both the ion drift velocity  $U_i$  and temperature  $T_i$  are independent of location. The approximate phase velocity for cold electrons  $\omega/k_y \approx U_i/2$  is shown in the shaded region. The essential point is the phase velocity is in the proper region to permit a resonant scattering of ions from the crossing region of phase space into the noncrossing region as illustrated at the bottom of Fig. 2. Although the reverse scattering is also possible, the slope of the distribution function in the vicinity of the resonance favors the process in Fig. 2. This type of scattering can only occur if the spatial extent of the crossing ion orbits  $\delta_i \approx \sqrt{2\rho_i L}$  overlaps with the spatial localization of the mode. It was recently proposed that this type of scattering may lead to the creation of significant shear in the ion velocity [25]. In the present context, the resonant scattering leads to a loss of positive charge in the center in conjunction with a gain in the edge region, and therefore gives rise to an electrostatic potential structure across the layer as shown in Fig. 1d.

To understand the increase in the electron flow velocity, consider the electron momentum equation within the fluid approximation. Neglecting the inertia term and using the equilibrium distribution to evaluate the pressure

tensor, the resulting electron flow velocity is

$$V_{ey} \approx \frac{U_e}{1 + (n_b/n_o) \cosh^2(z/L)} - \frac{c}{B_x} \frac{\partial \phi}{\partial z}, \quad (2)$$

The first term is the equilibrium flow while the second term is the  $\mathbf{E} \times \mathbf{B}$  drift induced by the electrostatic potential structure. At early times within the simulation, the electron velocity is in excellent agreement with Eq. (2) as shown in Fig. 1b, indicating the acceleration is a direct result of the electrostatic potential. As the simulation proceeds, the electron pressure tensor is strongly modified and the simple relationship in Eq. (2) is no longer accurate. The ion flow is also modified by the electrostatic potential, but to a much smaller degree due to the large inertia. It is important to emphasize, this physical mechanism for electron acceleration is very different than the results reported by Scholer [14] in which an inductive electric field is responsible for the acceleration while the electrostatic field is negligible. It does not appear this difference is due to the parameter regime in Ref. [14] since our simulations indicate the electrostatic potential continues to play an essential role at lower mass ratio but the bifurcated current structure is greatly diminished.

The anisotropic electron heating in the outer region  $|z/L| \gtrsim 0.7$  is a direct consequence of the LHDI due to the electron  $\nabla B$  drift resonance [6]. Clearly this mechanism is not relevant in the central region  $|z/L| < 0.7$  due to the absence of fluctuations. Since the nonlinear modification to the magnetic field occurs on the ion time scale, one approach to explain the heating is to examine the adiabatic invariants for the various electron orbits. For a system with periodic motion, the action integral taken over a period  $\oint p dq$  is a constant of the motion, where  $p$  and  $q$  are the generalized momentum and coordinate describing the periodic motion. When a change is imposed on the system so that the motion is no longer exactly periodic, the integral  $\oint p dq$  is an adiabatic invariant provided that the change is slow in comparison to the period of motion. For the case of noncrossing electrons with helical trajectories, the well-known magnetic moment  $\mu \equiv mv_\perp^2/(2B_x)$  is the relevant adiabatic invariant. This implies the perpendicular temperature is simply related to the local magnetic field

$$\frac{T_{e\perp}(z, t)}{T_{e\perp}(z, t=0)} \approx \frac{B_x(z, t)}{B_x(z, t=0)}. \quad (3)$$

For the region  $0.3 \lesssim |z/L| \lesssim 0.5$  where the electron orbits are helical, this expression provides a good estimate of the perpendicular heating as shown by the blue line in Fig. 1c. In the central region  $|z/L| < 0.3$ , the electron trajectories undergo a variety of complicated crossing orbits and  $\mu$  is no longer the relevant invariant. Approaches for constructing adiabatic invariants in regions of strong gradients [26] will be examined in future work.

These results demonstrate the essential physics of the nonlinear deformation at early time for realistic mass ratio. This process leads to a significant increase in

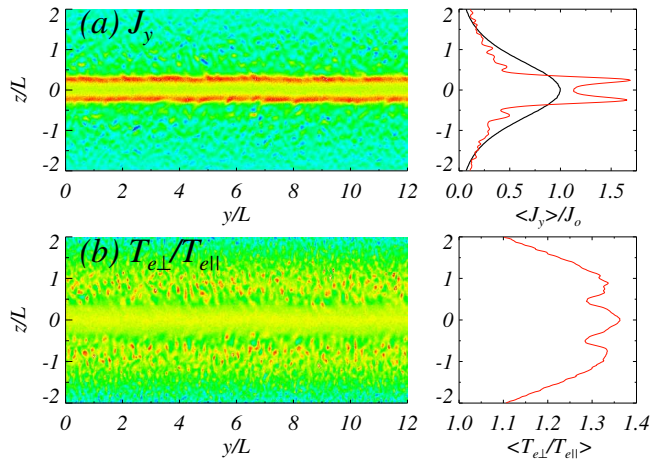


FIG. 3: Late time evolution for  $m_i/m_e = 512$  at  $t\Omega_{ci} = 29$  showing (a) current density  $J_y$  and (b) electron anisotropy  $T_{e\perp}/T_{e\parallel}$ . The  $y$ -averaged profiles (red) and initial current density (black) are shown on the right.

the electron velocity in the range  $|z/L| \lesssim 0.5$  and since the LHDI is driven by a relative drift between electrons and ions, one would expect the spatial region of wave activity to move inward. This in turn would lead to more ion scattering and further enhancements to the electrostatic potential, current bifurcation and electron anisotropy. Unfortunately, to confirm this scenario at realistic mass ratio is prohibitively expensive. However, longer simulations performed with the reduced mass ratio  $m_i/m_e = 512$  confirm this hypothesis. As shown

in Fig. 3 at time  $t\Omega_{ci} = 29$ , the peak current density increases by nearly 70% while the electron anisotropy reaches  $T_{e\perp}/T_{e\parallel} \approx 1.35$  in the central region.

In summary, the LHDI has been simulated for the first time at physically realistic mass ratio using a fully kinetic approach which resolves all relevant scales. For the initial sheet thickness  $\rho_i/L = 1$ , the modes are localized on the edge of the layer in agreement with linear theory. Nevertheless, the nonlinear evolution gives rise to a resonant scattering of crossing ions into the noncrossing region of phase space. This in turn produces an electrostatic potential structure across the layer leading to a strong bifurcation of the current density and perpendicular electron heating. The collisionless tearing mode is driven by the gradient of the current density [4], but is also very sensitive to the electron anisotropy [27, 28]. Thus the nonlinear development of the LHDI can dramatically increase the growth rate of tearing without invoking anomalous resistivity. For the parameters in this manuscript, the maximum tearing growth rate with isotropic electrons is  $\gamma/\Omega_{ci} \approx 0.035$  at  $k_x L \approx 0.45$ , while for  $T_{e\perp}/T_{e\parallel} \approx 1.1$  the growth rate increases to  $\gamma/\Omega_{ci} \approx 2.2$  with  $k_x L \approx 4$ . Simulations indicate the rapid growth and coalescence of small scale tearing islands can result in the onset of large scale reconnection [20]. This mechanism is activated when the current layer approaches a critical thickness  $\rho_i/L \approx 0.5$  where the crossing ion trajectories extend into the region of LHDI fluctuations.

This work was supported by the Los Alamos National Laboratory Directed Research and Development program (LDRD) and the NASA Geospace Sciences Program.

- 
- [1] V. Sergeev, D. G. Mitchell, C. T. Russell, and D. J. Williams, *J. Geophys. Res.* **98**, 17,345 (1993).
  - [2] V. Sergeev, V. Angelopoulos, C. Carlson, and P. Stutcliffe, *J. Geophys. Res.* **103**, 9177 (1998).
  - [3] M. Yamada, H. Ji, S. Hsu, T. Carter, R. Kulsrud, and F. Trintchouk, *Phys. Plasmas* **7**, 1781 (2000).
  - [4] B. Coppi, G. Laval, and R. Pellat, *Phys. Rev. Lett.* **16**, 1207 (1966).
  - [5] J. D. Huba, J. F. Drake, and N. T. Gladd, *Phys. Fluids* **23**, 552 (1980).
  - [6] R. C. Davidson, N. T. Gladd, C. S. Wu, and J. D. Huba, *Phys. Fluids* **20**, 301 (1977).
  - [7] D. Winske, *Phys. Fluids* **24**, 1069 (1981).
  - [8] M. Tanaka and T. Sato, *J. Geophys. Res.* **86**, 5541 (1981).
  - [9] S. Bale, F. Mozer, and T. Phan, *Geophys. Res. Lett.* **29**, 2180 (2002).
  - [10] I. Shinohara, T. Nagai, M. Fujimoto, T. Terasawa, T. Mukai, K. Tsuruda, and T. Yamamoto, *J. Geophys. Res.* **103**, 20365 (1998).
  - [11] T. Carter, J. Ji, F. Trintchouk, M. Yamada, and R. Kulsrud, *Phys. Rev. Lett.* **88**, 5001 (2002).
  - [12] R. Horiuchi and T. Sato, *Phys. Plasmas* **6**, 4565 (1999).
  - [13] G. Lapenta and J. U. Brackbill, *Phys. Plasmas* **9**, 1544 (2002).
  - [14] M. Scholer, I. Sidorenko, C. Jaroscheck, R. Treumann, and A. Zeiler, *Phys. Plasmas* **10**, 3521 (2003).
  - [15] P. Pritchett, in *Proceedings of the ICS-6*, edited by R. Winglee (Univ. of Washington, Seattle, 2002), p. 225.
  - [16] H. Ji, S. Terry, M. Yamada, R. Kulsrud, A. Kuritsyn, and Y. Ren, *Phys. Rev. Lett.* **92**, 115001 (2004).
  - [17] W. Daughton, *Phys. Plasmas* **10**, 3103 (2003).
  - [18] A. Runov, R. Nakamura, W. Baumjohann, T. Zhang, M. Volwerk, H.-U. Eichelberger, and A. Balogh, *Geophys. Res. Lett.* **30**, 1036 (2003).
  - [19] V. Sergeev, A. Runov, W. Baumjohann, R. Nakamura, T. Zhang, M. Volwerk, A. Balogh, H. Reme, J. Sauvaud, M. Andre, et al., *Geophys. Res. Lett.* **30**, 1327 (2003).
  - [20] P. Ricci, J. Brackbill, W. Daughton, and G. Lapenta, submitted to *Phys. Plasmas* (2004).
  - [21] E. G. Harris, *Nuovo Cimento* **23**, 115 (1962).
  - [22] A. Lui, in *Magnetotail Physics*, edited by A. Lui (John Hopkins Univ. Press, Baltimore, 1987), p. 3.
  - [23] R. Morse and C. Nielson, *Phys. Fluids* **14**, 830 (1971).
  - [24] D. Forslund, in *Space Plasma Simulations*, edited by M. Ashour-Abdalla and D. Dutton (D. Reidel, Norwell, Mass., 1985), pp. 425–439.
  - [25] W. Daughton, *Phys. Plasmas* **9**, 3668 (2002).
  - [26] E. Whipple, *J. Geophys. Res.* **91**, 4149 (1986).
  - [27] D. Forslund, *Ph.D. thesis* (Princeton University, 1968).
  - [28] J. Chen and P. Palmadesso, *Phys. Fluids* **27**, 1198 (1984).